Research Square

Preprints are preliminary reports that have not undergone peer review.
They should not be considered conclusive, used to inform clinical practice,
or referenced by the media as validated information.

# Genome-Wide Identification, Expression Profiling, and Stress Responses of the Sugar Transporter Gene Family in Tomato (Solanum lycopersicum)

**Zijian Liu**
China Agricultural University
**Yafeng Gu**
China Agricultural University
**Xingyi Wang**
China Agricultural University
**Lingyan Shen**
Zhangjiakou Academy of Agricultural Sciences
**Yuxi Tang**
China Agricultural University
**Xin Li**
China Agricultural University
**Yongqiang Tian**
China Agricultural University
**Si Ma**
masi@cau.edu.cn

China Agricultural University

**Research Article**

**Keywords:** Tomato (Solanum lycopersicum), Sugar Transport Protein (STP), Phylogenetic analysis, Tissue-specific expression, Abiotic/biotic stress

**Posted Date:** October 29th, 2026

**DOI:** https://doi.org/10.21203/rs.3.rs-11326952/v1

**License:** This work is licensed under a Creative Commons Attribution 4.0 International License. Read Full License

**Additional Declarations:** No competing interests reported.

## Abstract

The Sugar Transporter Protein (STP) family mediates monosaccharide transport and plays essential roles in plant development and stress responses, yet systematic analysis in tomato remains limited. Here, we analyzed the 18 previously reported SlSTPs. Phylogeny classified them into four clades designated Clade I, Clade II, Clade III and Clade IV, with Clade I absent in tomato. Tandem duplications on chromosome 3 drove family expansion. Conserved motifs and gene structures showed clade-specific conservation. Promoters contained abundant light-responsive, hormone-responsive and stress-responsive cis-elements. Tissue expression revealed that *SlSTP1*, *SlSTP12* and *SlSTP16*, which belong to Clade II, were predominantly expressed in roots, while *SlSTP9* and *SlSTP11* of Clade III were flower-specific; most genes were only detectable during early fruit development. Under nematode infection, *SlSTP1*, *SlSTP2*, *SlSTP3*, *SlSTP8* and *SlSTP12* peaked at 21 days post inoculation, coinciding with the giant-cell stage. Under drought, salt and heat stresses, *SlSTP7* and *SlSTP12* showed broad responses; *SlSTP6* and *SlSTP12* were strongly induced in roots under drought stress, with $\log_2$ fold changes exceeding 5. *SlSTP2* was nematode-specific, whereas *SlSTP5*, *SlSTP*9 and *SlSTP17* responded only to abiotic stresses. This study provides candidate genes for improving sugar metabolism and stress tolerance in tomato.

## Introduction

Sugars are central energy sources and structural components in plant cells, participating not only in fundamental physiological processes such as carbohydrate metabolism, cell proliferation, and differentiation, but also acting as signaling molecules that regulate growth and development, stress responses, and secondary metabolism (Chen et al., 2015). The distribution and homeostasis of glucose, fructose, sucrose, and other sugars in plants rely on transmembrane transport mediated by sugar transporters. Among them, the sugar transporter (STP) family is specifically mediates for the transmembrane transport of monosaccharides such as glucose, galactose, and mannose, playing indispensable roles in nutrient uptake, organogenesis, stress adaptation, and immune defense (Afoufa-Bastien et al., 2010; Büttner, 2010; Geiger, 2020).

The STP family belongs to the Major Facilitator Superfamily (MFS), with members universally possessing 12 conserved transmembrane domains that provide the structural basis for plasma membrane $H^+$/monosaccharide symport (Büttner, 2010). Genome-wide identification of *STP* families has been conducted in Arabidopsis (*Arabidopsis thaliana*), rice (*Oryza sativa*), maize (*Zea mays*), tomato (*Solanum lycopersicum*), potato (*Solanum tuberosum*), and several Brassica crops, revealing pronounced tissue-specific expression and functional divergence among members (Büttner, 2010; Reuscher et al., 2014; Liu et al., 2018; Kong et al., 2019; Zhang et al., 2019; Wei et al., 2020; Liu et al., 2021, 2022; Xiao et al., 2022; Ma et al., 2023; Devi et al., 2025; Mia et al., 2025). In *Arabidopsis*, *AtSTP1* exerts dual roles in root monosaccharide uptake and guard cell osmoregulation, *AtSTP2/6/9/11* are specifically expressed during pollen development and tube growth, and *AtSTP4* and *AtSTP13* are implicated in wound/pathogen responses and programmed cell death, respectively (Büttner, 2010). In crops, multiple *OsSTP* members in rice respond to heat, salt, and osmotic stresses, *ZmSTP2/20* in maize contribute to broad-spectrum disease resistance, and *StSTP10/12* in potato maintain sugar transport homeostasis under drought and low-temperature stress (Kong et al., 2019; Ma et al., 2023; Mia et al., 2025). Collectively, these findings have established an important foundation for understanding the evolutionary patterns and functional conservation of the plant *STP* family.

Tomato is both a globally important economic crop and a model system for fleshy fruit development, with fruit quality and yield highly dependent on the transport and accumulation of glucose and fructose. However, tomato production is frequently threatened by abiotic stresses such as salinity, drought, and extreme temperatures, as well as biotic stresses including pathogens and nematodes, all of which disrupt sugar metabolism and compromise yield (Caseys, 2018; Bhattarai et al., 2021; Reimer et al., 2021). Although *STP* family functions have been extensively characterized in model plants such as *Arabidopsis*, systematic investigation of the *SlSTP* family in tomato remains limited, with only a few members functionally explored: *SlSTP1* participates in fruit sugar accumulation and quality regulation (Wang et al., 2023); *SlSTP2* is pathogen-inducible and positively regulates tomato resistance to bacterial leaf spot, representing an important immune regulator (Li et al., 2022) ; *SlSTP10* is induced upon root-knot nematode infection and modulates root sugar allocation to shape tomato susceptibility to root-knot nematodes(Sun et al., 2024). Thus, genome-wide identification and functional characterization of the *STP* family in tomato are of considerable scientific significance and practical value.

In this study, based on previously published 18 *SlSTP* sequences (Reuscher et al., 2014), we performed comprehensive bioinformatic analyses including phylogenetic relationship, chromosomal distribution, gene structure, conserved motifs, and promoter cis-acting elements. qRT-PCR was used to explore tissue-specific expression profiles and transcriptional responses to drought, salt, heat and root-knot nematode infection. This work systematically supplements the research of *SlSTP* family and provides valuable candidate genes and theoretical reference for molecular breeding targeting fruit sugar improvement and stress tolerance enhancement in tomato.

## Materials and Methods

**Identification of SlSTP Family**

Based on the gene IDs of all *SlSTP* reported by Reuscher et al. (2014), the tomato reference genome sequence and its corresponding genome annotation file (GFF3 format, version ITAG 3.2) were downloaded from the Phytozome database (https://phytozome-next.jgi.doe.gov/) and Sol Genomics Network (SGN, https://solgenomics.net/).

**Chromosomal Physical Mapping of SlSTP Family**

The physical map was constructed using TBtools software. Based on the chromosome length information from the ITAG 3.2 annotation file, the vertical skeletons of 12 core tomato chromosomes (ch01–ch12) were drawn. The physical positions of the 18 identified *SlSTP* were imported and annotated at their corresponding chromosomal loci. The gene distribution density across the entire tomato genome was calculated using a 1 Mb sliding window with the "Gene

Density Profile" function of TBtools. The color gradient (from blue to green) inside the bars reflects the gene density in that chromosomal segment. The physical scale bar on the left was set to megabases (Mb), with a maximum range of 100 Mb. A high-resolution physical localization map was subsequently exported.

# Prediction of Physicochemical Properties, Conserved Motifs and Gene Structures of SlSTP

The basic physicochemical parameters including molecular weight, theoretical isoelectric point (pI), instability index, aliphatic index and grand average of hydropathicity (GRAVY) of each SlSTP were predicted via ExPASy ProtParam (https://web.expasy.org/). Conserved motifs of *SlSTP* were analyzed using MEME Suite (https://meme-suite.org/meme/tools/meme). The exon-intron structural information was obtained from genome annotation files and visualized by GSDS 2.0 online tool.Signal peptide prediction was performed using TargetP-2.0 online server; transmembrane helices were predicted via TMHMM Server v.2.0 (https://services.healthtech.dtu.dk/services/TMHMM-2.0/); subcellular localization of each SlSTP was analyzed by DeepLoc 2.1 webserver (https://services.healthtech.dtu.dk/services/DeepLoc-2.1/).

## Secondary Structure Prediction of SlSTP

The secondary structure components including α-helix, extended strand, β-turn and random coil of all 18 SlSTP were calculated on SOPMA webserver (https://npsa.lyon.inserm.fr/cgi-bin/npsa_automat.pl?page=/NPSA/npsa_sopma.html) under default parameters, and corresponding structural sketch maps were generated.

## Homology Modeling of Tertiary Structure

Homology-based three-dimensional structural modeling of 18 SlSTP was accomplished on the SWISS-MODEL platform (https://swissmodel.expasy.org/). The server automatically screened suitable homologous crystal templates from PDB database for model construction.

## Phylogenetic Tree Construction of STP Family from Multiple Species

Tomato (*Solanum lycopersicum*, ITAG 3.2) sequences were downloaded from the Phytozome database (https://phytozome-next.jgi.doe.gov/); potato (*Solanum tuberosum*, SolTub_3.0) from the Sol Genomics Network (SGN) database (https://solgenomics.net/); Arabidopsis (*Arabidopsis thaliana*, TAIR10) from The *Arabidopsis* Information Resource (TAIR) database (https://www.arabidopsis.org/); rice (*Oryza sativa*, v7.0) from the Ensembl Plants database (https://plants.ensembl.org/); and maize (*Zea mays*, APGv4) from the Phytozome database.

Full-length protein sequences of all identified STP members were aligned using the MUSCLE Wrapper tool in TBtools v1.120. The alignment results were trimmed using the Simple MSA Trimmer function with a site coverage cutoff of 0.5, which removes sites with deletions in 50% or more of the sequences. An unrooted phylogenetic tree was constructed using the maximum likelihood method with the IQ-TREE plugin integrated in TBtools under the LG + G+I model, and branch reliability was assessed with 1,000 bootstrap replicates.

**Interspecies Collinearity Analysis of SlSTP**

Genome-wide alignment of tomato protein sequences against protein sequences from other species was performed using BLASTP (E-value < $1\times e^{-5}$). Gene duplication events and interspecies collinearity relationships were subsequently analyzed using TBtools integrated with the Multiple Collinearity Scan toolkit (MCScanX). Visualization was conducted using the Dual Synteny Plot module in TBtools. Relevant genome data were retrieved from NCBI database (https://www.ncbi.nlm.nih.gov/).

**Cis-acting Element Analysis of SlSTP**

The 2000 bp upstream sequences of the translation initiation codon of each *SlSTP* were extracted from the tomato reference genome (SL3.2) using the "GXF Sequences Extract" function of TBtools, based on the ITAG 3.2 annotation file. Cis-acting elements in the promoter sequences were predicted using the PlantCARE database. Elements related to plant growth and development, hormone responses (auxin, gibberellin, abscisic acid, jasmonic acid, etc.), and biotic/abiotic stresses (nematode, drought, salt, low temperature, etc.) were screened. The distribution of cis-acting elements was visualized using TBtools, and the number and distribution characteristics of different types of elements were statistically analyzed.

**Tissue-specific Expression Profiling of SlSTP**

The expression data of the 18 *SlSTP* in 10 tissues and developmental stages (Root, Leaves, Unopened Flower Bud, Fully Opened Flower, 1 cm Fruit, 2 cm Fruit, 3 cm Fruit, Mature Green Fruit, Breaker Fruit, and Breaker Fruit + 10 days) were downloaded from the Tomato eFP Browser (http://bar.utoronto.ca/efp_tomato/). The original FPKM values were normalized using the $\log_2(x + 1)$ method. The normalized data were imported into GraphPad Prism 8 to generate an expression heatmap.

## Nematode Inoculation and Sample Collection

*Meloidogyne incognita* was propagated on water spinach (*Ipomoea aquatica*). Nematode eggs were separated from infected root tissues and incubated at 28 ℃ to hatch into active second-stage juveniles (J2). After counting and gradient dilution, a uniform nematode suspension was prepared, and each seedling was inoculated with 600 active J2 via root irrigation. Uniform seedlings at early flower bud stage with 6–7 fully expanded true leaves were selected, the experiment was set up with three independent biological replicates. Root samples were collected at 7, 14, 21, 28 and 35 days post inoculation, immediately frozen in liquid nitrogen and stored at − 80 ℃ for subsequent total RNA extraction and qRT-PCR detection. Expression fold changes were calculated as $\log_2$(inoculated/control) for heatmap plotting.

# Abiotic Stress Treatment and Sample Collection

Seedlings at early flower bud stage with 6–7 fully expanded true leaves were separated into four groups: normal control irrigated with clean water, 20% PEG6000 drought treatment, 200 mM NaCl salt treatment and high-temperature (38 ℃ for 30 min) treatment. The whole experiment was performed with three independent biological replicates. All seedlings were cultured in growth chambers at 25 ℃ with consistent humidity and 16 h light / 8 h dark photoperiod. Each group was irrigated with 50 mL of the corresponding solution daily for 8 consecutive days, and different plant tissues (roots, stems, leaves and flowers) were collected at the end of the treatment period. Collected samples were immediately frozen in liquid nitrogen and stored at − 80 ℃ for subsequent RNA extraction and qPCR detection. The relative expression values of stress-treated groups were calculated as $\log_2$(treatment/control) for heatmap construction.

## RNA Extraction and Quality Control

Total RNA was extracted from all collected plant tissue samples using the Plant Total RNA Extraction Kit (Promega, Shanghai, China) strictly following the manufacturer's instructions. The concentration and purity of total RNA were determined using a NanoDrop 2000 spectrophotometer (Thermo Fisher Scientific, USA), and RNA integrity was verified by 1% agarose gel electrophoresis. Only RNA samples with $A_{260}/A_{280}$ ratio between 1.8 and 2.1 and clear 28S/18S rRNA bands were used for subsequent experiments.

## First-Strand cDNA Synthesis

Qualified RNA was reversely transcribed into first-strand cDNA with Evo M-MLV reverse transcription kit (Accurate Biology, China). The total 20 μL reverse transcription reaction system contained 1 μg total RNA, 2 μL gDNA Clean Reaction Mix Ver.2, 4 μL 5× Evo M-MLV RT Mix, and RNase-free dd$H_2O$ supplemented to a final volume of 20 μL. The reverse transcription reaction was performed according to the following program: 37 ℃ for 15 min, 85 ℃ for 5 s, and incubation at 4 ℃ for storage. The obtained cDNA product was stored at − 20 ℃ for subsequent qPCR detection.

# Primer Design and Synthesis

Specific primers for all 18 *SlSTP* were designed using Primer Premier 5.0 software based on their coding sequences. *SlActin2* (Solyc11g005330) was selected as the internal reference gene. All primers were synthesized by Beijing Youkang Biotechnology Co., Ltd., and the primer sequences are listed in Supplementary Table S1.

# RT-qPCR Amplification and Data Analysis

RT-qPCR was performed on a CFX96 Real-Time PCR System (Bio-Rad, USA) using Novozan SYBR Green Pro Taq HS qPCR Mix (Cat. Q311-02). The total 10 μL qPCR reaction system contained 5 μL 2× SYBR Green Pro Taq HS qPCR Mix, 0.2 μL forward primer (10 μM), 0.2 μL reverse primer (10 μM), 2 μL cDNA template, and 2.6 μL RNase-free dd$H_2O$. The amplification procedure was as follows: pre-denaturation at 95 ℃ for 30 s; 40 cycles of denaturation at 95 ℃ for 5 s and annealing/extension at 60 ℃ for 30 s; followed by melting curve analysis (95 ℃ for 15 s, 60 ℃ for 1 min, 95 ℃ for 15 s). Three technical replicates were set for each sample, and the relative expression levels of *SlSTP* were calculated using the $2^{-\Delta\Delta Ct}$ method.

# Software and tools

Excel 2019 for raw data sorting and statistics; DNAMAN 9.0 and GeneDoc for multiple sequence alignment; GSDS 2.0 for gene structure visualization; TBtools v1.120 for chromosomal mapping, phylogenetic tree construction, collinearity analysis, *cis*-acting element prediction and whole-genome data processing; GraphPad Prism 8 for heatmap generation; Adobe Illustrator for figure polishing and layout.

## Results

**Genome-wide physicochemical analysis of the SlSTP family**

Based on the gene IDs reported by Reuscher et al. (2014), the protein sequences of 18 SlSTP were retrieved from the ITAG 3.2 tomato reference genome. Previous researches have confirmed that all sequences contain intact Sugar conserved domains, so conserved domain identification was not repeated in this work, and all physicochemical parameters are listed in Table 1. The deduced amino acid lengths of SlSTP ranged from 267 aa (SlSTP17) to 715 aa (SlSTP9), with corresponding molecular weights of 29.93 kDa–78.13 kDa. All proteins had alkaline Isoelectric point values ranging from 8.68 to 9.96 with an average of 9.17, which was obviously different from the acidic property of STP homologs from Brassicaceae. Positive values of Grand Average of Hydropathicity (GRAVY) across the entire family verified their hydrophobic properties, matching the typical characteristics of the Major Facilitator Superfamily (MFS) transporters. High aliphatic index suggested good thermal stability. Fifteen proteins had an instability index below 40 and were classified as stable proteins, while SlSTP4/8/17 showed slightly higher values and relatively poorer stability. Prediction results demonstrated that none of the SlSTP contained N-terminal

signal peptides, whereas all possessed canonical transmembrane helices. As integral MFS-type membrane proteins, SlSTP anchor biomembranes via transmembrane segments, which was consistent with previous structural reports of STP in other Solanaceae plants. Subcellular localization prediction was highly consistent with structural traits: fifteen proteins were exclusively localized on plasma membrane, and SlSTP2, SlSTP14, SlSTP16 were dual-targeted to plasma membrane and vacuole/lysosome, implying their dual roles in extracellular monosaccharide uptake and vacuolar sugar storage to maintain intracellular sugar homeostasis. Taken together, SlSTP family members exhibit canonical structural features of plant monosaccharide transporters, laying a solid foundation for subsequent phylogenetic, *cis*-element and expression-related researches.

Table 1
Information about the *SlSTP*

| Gene name | Gene ID | Protein length (aa) | Molecular weight (kD) | Isoelectric point | Grand average of hydropathicity | Aliphatic index | Instability index | Signal peptide | Transmem-brane | Subcellular localization |
|---|---|---|---|---|---|---|---|---|---|---|
| *SlSTP1* | Solyc02g079220 | 523 | 57.86 | 9.15 | 0.543 | 106.08 | 31.29 | No | Yes | Cell membrane |
| *SlSTP2* | Solyc09g075820 | 523 | 57.58 | 9.03 | 0.487 | 109.02 | 35.76 | No | Yes | Cell membrane Lysosome/Vac |
| *SlSTP3* | Solyc07g006970 | 572 | 63.36 | 9.80 | 0.465 | 109.62 | 39.62 | No | Yes | Cell membrane |
| *SlSTP4* | Solyc04g074070 | 509 | 55.55 | 9.45 | 0.531 | 102.53 | 44.79 | No | Yes | Cell membrane |
| *SlSTP5* | Solyc01g010530 | 489 | 54.13 | 9.01 | 0.664 | 110.43 | 32.28 | No | Yes | Cell membrane |
| *SlSTP6* | Solyc08g080300 | 528 | 58.15 | 9.15 | 0.512 | 102.46 | 27.27 | No | Yes | Cell membrane |
| *SlSTP7* | Solyc03g005140 | 487 | 53.82 | 9.25 | 0.630 | 110.31 | 32.38 | No | Yes | Cell membrane |
| *SlSTP8* | Solyc00g009030 | 426 | 47.09 | 9.01 | 0.375 | 102.09 | 42.07 | No | Yes | Cell membrane |
| *SlSTP9* | Solyc01g008240 | 715 | 78.13 | 9.01 | 0.413 | 100.45 | 30.94 | No | Yes | Cell membrane |
| *SlSTP10* | Solyc03g006650 | 518 | 56.90 | 8.80 | 0.564 | 107.47 | 26.19 | No | Yes | Cell membrane |
| *SlSTP11* | Solyc06g054270 | 489 | 53.69 | 8.91 | 0.653 | 108.65 | 34.26 | No | Yes | Cell membrane |
| *SlSTP12* | Solyc05g018230 | 516 | 56.67 | 8.87 | 0.476 | 104.75 | 36.79 | No | Yes | Cell membrane |
| *SlSTP13* | Solyc03g005150 | 487 | 53.59 | 9.60 | 0.638 | 109.34 | 26.88 | No | Yes | Cell membrane |
| *SlSTP14* | Solyc03g078600 | 462 | 51.32 | 8.68 | 0.656 | 109.07 | 31.59 | No | Yes | Cell membrane Lysosome/Vac |
| *SlSTP15* | Solyc03g093400 | 702 | 76.03 | 9.96 | 0.396 | 104.15 | 37.77 | No | Yes | Cell membrane |
| *SlSTP16* | Solyc03g093410 | 514 | 55.91 | 9.34 | 0.604 | 107.57 | 34.01 | No | Yes | Cell membrane Lysosome/Vac |
| *SlSTP17* | Solyc03g094170 | 267 | 29.93 | 9.30 | 0.356 | 104.08 | 40.65 | No | Yes | Cell membrane |
| *SlSTP18* | Solyc12g008320 | 515 | 56.48 | 8.92 | 0.557 | 109.50 | 32.17 | No | Yes | Cell membrane |

**Chromosomal Physical Mapping of the SlSTP Family**

The physical map of *SlSTP* was constructed via TBtools using SL3.0 tomato reference genome and ITAG 3.2 gene annotation. SL3.0ch00 corresponds to unanchored scaffold sequences that cannot be assigned to the 12 canonical chromosomes (ch01–ch12). The 18 *SlSTP* displayed uneven chromosomal distribution across SL3.0ch00, ch01–ch09 and ch12, whereas no *SlSTP* were found on ch10 and ch11 (Fig. 1). Specifically, one *SlSTP* (*SlSTP8*) was located on SL3.0ch00; two *SlSTP* (*SlSTP5/9*) mapped to ch01; ch03 contained seven members (*SlSTP7/10/13/14//15/16/17*), accounting for 38.9% of total family members. Each of ch02, ch04, ch05, ch06, ch07, ch08, ch09 and ch12 harbored a single *SlSTP*, namely *SlSTP1, SlSTP4, SlSTP12, SlSTP11, SlSTP3, SlSTP6, SlSTP2, SlSTP18*, respectively. Two distinct tandem gene clusters were identified on ch03: *SlSTP7/13/10* clustered closely at the terminal region, while *SlSTP14/15/16/17* formed another compact cluster in the middle-lower chromosomal region (Fig. 1). The clustered distribution pattern strongly indicates that tandem duplication is an essential evolutionary factor contributing to the expansion of *SlSTP* family.

**Phylogenetic and Interspecific Collinearity Analysis of the SlSTP Family**

To explore the evolutionary characteristics of *SlSTP*, STP sequences from five species including *Solanum lycopersicum*, *Solanum tuberosum*, *Arabidopsis thaliana*, *Oryza sativa* and *Zea mays* were used to construct an unrooted phylogenetic tree. All STP sequences were clustered into four evolutionary clades (Clade I–Clade IV), and all 18 SlSTP were distributed in Clade II, Clade III and Clade IV, while no tomato genes were identified in Clade I (Fig. 2a; Supplemental table S2). Evolutionary distance analysis revealed that SlSTP clustered closely with orthologous StSTP with short branch lengths of 0.01–0.03 and formed well-supported sister branches (e.g. SlSTP1/StSTP1, SlSTP7/StSTP13), which proved the close phylogenetic relationship and high sequence conservation of orthologous STP after Solanaceae speciation. The branch lengths between tomato and *Arabidopsis* ranged from 0.1 to 0.5, consistent with eudicot divergence, whereas values of 0.3 to 0.8 between tomato and rice/maize reflected the ancient divergence between monocots and eudicots. OsSTP25 had a branch length of 10.01, which was markedly different from other sequences.

To further explore the origin and evolutionary mechanism of *SlSTP*, genome-wide interspecific collinearity analysis was performed among three representative species including potato, *Arabidopsis* and rice, and the abundance of collinear blocks was closely associated with phylogenetic relatedness. Dense collinear regions and numerous syntenic *SlSTP - StSTP* pairs were identified between tomato and potato, demonstrating conserved chromosomal locations of STP during Solanaceae differentiation. Partial collinear fragments between tomato and *Arabidopsis* suggest that the STP family originated from the common ancestor of eudicots, whereas only sparse collinear genes were found between tomato and monocot rice, accompanied by drastically reduced positional conservation of STP along increasing evolutionary divergence (Fig. 2b).

**Gene Structure and Conserved Motif Analysis of the SlSTP Family**

Structural and motif analysis of *SlSTP* is displayed in Fig. 3. Divergent exon-intron organizations were observed across 18 *SlSTP*. Seven genes (38.9%), namely *SlSTP2/6/9/13/14/15/18*, contain four exons and three introns; three genes (*SlSTP3/7/17*) possess three exons and two introns; six genes (*SlSTP1/4/5/11/12/16*) carry five exons with variable intron numbers ranging from four to five; *SlSTP10* has six exons and five introns, while *SlSTP8* owns the simplest architecture with only one exon and one intron (Fig. 3). Genes clustered within identical phylogenetic clades share highly similar exon-intron composition and arrangement, revealing tight correlation between phylogenetic relatedness and structural conservation.

Ten distinct conserved motifs (Motif1–Motif10) were identified across the whole gene family. All ten motifs are generally conserved among *SlSTP*, yet partial genes lose one or several individual motifs or display altered motif arrangement, especially *SlSTP17* with severe motif deletion, as well as abnormal motif constitution in *SlSTP8/9/15*. Domain annotation indicated three main conserved domains including MFS_*STP*, CnoX and MFS superfamily, among which MFS_*STP* and MFS superfamily domains serve as characteristic functional motifs for *STP* (Fig. 3b).

# Analysis of Transmembrane Topology, Secondary and Tertiary Structures of SlSTP

The transmembrane topology of 18 SlSTP was predicted using the TMHMM 2.0 server. As shown in Table 1, no N-terminal signal peptide was detected in any of these proteins, which is consistent with the properties of typical membrane transporters. The number of predicted transmembrane helices (TMHs) varied substantially among family members (Supplementary Table S3). Eight members including SlSTP1/2/3/6/10/12/15/16 contained 12 TMHs, which is the canonical topological structure of the major facilitator superfamily (MFS) transporters. SlSTP4/5/7/9/11/13 had 11 TMHs, indicating slight deletion of transmembrane regions. SlSTP18 possessed 10 TMHs, while SlSTP14 (9 TMHs) and SlSTP8 (8 TMHs) exhibited obvious loss of transmembrane segments. Notably, SlSTP17 only had 4 TMHs. Combined with its extremely short protein length of 267 amino acids (Table 1), we confirmed that SlSTP17 is a severely truncated protein with massive deletion of transmembrane domains. In contrast, SlSTP9 (715 aa) and SlSTP15 (702 aa) had extraordinarily long amino acid sequences but retained normal numbers of transmembrane helices, demonstrating that their extra amino acid residues were distributed in intracellular and extracellular regions rather than transmembrane domains.

The secondary structure composition of all SlSTP was statistically analyzed based on prediction results (Supplementary Table S3). The proportion of α-helix, extended strand, β-turn and random coil differed across individual proteins. SlSTP17 had the highest α-helix content at 55.43% within the family. Combined with its dramatic reduction in transmembrane helices, this result suggested that most α-helices of SlSTP17 no longer performed transmembrane functions, leading to distinct spatial distribution of secondary structural elements. SlSTP8 and SlSTP14 also showed altered secondary structure features corresponding to their incomplete transmembrane topology.

Homology modeling of the tertiary structure was performed using the SWISS-MODEL platform. All constructed models had a GMQE value higher than 0.7 and reasonable QMEAN scores, verifying the reliability of the predicted three-dimensional structures (Fig. 4). Most SlSTP adopted the typical folding pattern of MFS transporters. Twelve transmembrane α-helices assembled to form an intact substrate-binding pocket and transmembrane channel, and the N- and C-terminal domains presented pseudo-twofold symmetry, which is the structural basis for recognizing and transporting monosaccharide substrates. However, the partial loss of transmembrane helices in SlSTP8/14/17 changed their overall spatial skeletons. The incomplete substrate-binding pocket and transport channel caused by transmembrane domain defects may impair monosaccharide transport capacity and eventually result in functional attenuation or functional differentiation of these three proteins.

**Analysis of Cis-Acting Regulatory Elements in Promoters of SlSTP**

To explore the transcriptional regulation of *SlSTP* and their roles in plant development and environmental adaptation, 2000 bp promoter sequences upstream of the ATG start codon from 18 *SlSTP* were subjected to cis-element prediction using PlantCARE. The element distribution and quantitative statistics are presented in Fig. 5a and 5b. All predicted cis-elements were classified into four major groups: light-responsive, phytohormone-responsive, stress-responsive and development-related elements. We further characterized three functional subgroups, namely heat shock-related, sugar signaling-related, and flower/fruit development-related cis-elements.

Light-responsive motifs were the most ubiquitous and abundant in all promoters, including G-box, Box 4, I-box, TCT-motif, AE-box and AT1-motif. As a multifunctional element, G-box also participates in sugar signal transduction and carbon metabolism. Every *SlSTP* contained more than two kinds of light-related elements, demonstrating that light serves as a crucial environmental signal modulating the global transcription of the *SlSTP* family.

Diverse hormone-responsive cis-elements were identified, such as ABRE (ABA), CGTCA-motif/TGACG-motif (MeJA), TCA-element (salicylic acid), TGA-element/AuxRR-core (auxin), GARE-motif and P-box (gibberellin) (Fig. 5b). These hormone-related motifs also act as key regulators of flower differentiation and fruit growth. Variations in element category and copy number among individual genes suggested distinct hormone responsiveness across family members.

Stress-related elements contained drought-inducible MBS, cold-responsive LTR, anaerobic-induced ARE, as well as defense-associated TC-rich repeats, W-box and WUN-motif. In addition, typical heat stress-related elements including ACE and STRE were detected (Fig. 5b). LTR and TC-rich repeats can also respond to high temperature, jointly mediating heat stress adaptation. *SlSTP2* and *SlSTP5* possessed remarkably abundant stress motifs, implying their essential functions against drought, low temperature, waterlogging and heat stress.

Development-associated elements involved CAT-box for meristem-specific expression, O2-site for endosperm development and sugar accumulation, circadian-control motifs, flavonoid biosynthesis-related chs-CMA1a and various transcription factor binding sites. GARE-motif, P-box, GA-motif, TGA-element and AuxRR-core regulate flower organogenesis and fruit expansion. These cis-elements collectively participate in meristem differentiation, flower development, fruit growth, seed development and secondary metabolism in tomato.

**Spatiotemporal Expression and Responses to Various Stresses of SlSTP**

Transcript data across different tissues and developmental stages showed distinct tissue-preferred expression patterns of the *SlSTP* family (Fig. 6a). Most genes accumulated high transcripts in flower buds and decreased after anthesis, while *SlSTP9/11* kept high expression from budding to full bloom. *SlSTP1/12/16/17* were mainly expressed in roots, and *SlSTP7* had moderate root expression. Overall expression was low in leaves, with relatively high levels for *SlSTP1/2/15/17*. Most members presented low transcription during fruit development: *SlSTP9/11/13/16* maintained low expression throughout fruit growth; *SlSTP1* was transiently induced in 1–3 cm young fruits, *SlSTP3* had stable moderate expression, and *SlSTP10* peaked only at the 1 cm fruit stage.

*SlSTP* exhibited stage-dependent expression alterations upon root-knot nematode inoculation (Fig. 6b). Only *SlSTP*10 was upregulated at 7–14 dpi; *SlSTP*1/2/3/8/12 reached expression peaks synchronously at 21 dpi. Most induced genes returned to basal levels at 28–35 dpi, whereas *SlSTP*13 was specifically upregulated at 35 dpi. *SlSTP*16 was continuously suppressed during the whole infection period with the lowest expression at 35 dpi.

Drought, salt and heat induced tissue-specific expression changes of *SlSTP* (Fig. 6c–e). *SlSTP7/12* were induced under all three stresses: *SlSTP7* was upregulated in roots and leaves, and *SlSTP12* exhibited variable induction across tissues under different stresses. Drought induced prominent upregulation of *SlSTP6/7/12/14/16* in roots, while few genes changed in flowers. Salt altered transcription largely in roots and flowers; *SlSTP12* increased in roots and flowers, *SlSTP6* in leaves and *SlSTP17* in roots. Heat triggered differential expression across organs: *SlSTP10* was induced in roots and leaves, whereas *SlSTP17* was downregulated in roots yet upregulated in flowers.

## Discussion

**Inter-species Variation of Gene Number and Lineage-Specific Evolutionary Divergence of SlSTP**

The 18 *SlSTP* used in the present study were obtained from published research by Reuscher et al. (2014). Dramatic copy-number variation of *STP* was observed across different plant taxa: two Solanaceae relatives, potato and pepper, possess 21 and 17 *STP* respectively (Wei et al., 2020; Mia et al., 2025). Within Brassicaceae, *Arabidopsis thaliana* contains only 14 *STP* members (Büttner, 2010), while *Brassica oleracea var. capitata* expands to 22 copies (Zhang et al., 2019). In monocots, rice and maize harbor 28 and 22 *STP* individually (Kong et al., 2019). Such numerical divergence reflects lineage-specific expansion of the *STP* family triggered by polyploidization and genome rearrangement after the divergence of monocots and dicots. Phylogenetic analysis categorized STP from tomato, potato, *Arabidopsis*, rice and maize into four clades (Clade I–IV). Clade I is monocot-exclusive and only consists of rice and maize homologs, whereas no dicot genes from tomato, potato or *Arabidopsis* fall into this clade, with all 18 SlSTP restricted to Clade II, III and IV (Fig. 2a). This topology indicates Clade I expanded specifically in monocot lineages after monocot–dicot split, while dicots lost this clade in early evolution. It is proposed that tomato discarded Clade I genes during Solanaceae evolution, and the original biological functions of Clade I concerning specialized monosaccharide transport and stress adaptation have been functionally compensated by other SlSTP subgroups or distinct sugar transporter families, forming the unique evolutionary profile of SlSTP family.

**Conserved Gene Structure, Motif Characteristics and Tandem Duplication-Mediated Expansion & Functional Diversification of SlSTP**

Exon-intron organizations of *SlSTP* diverge considerably. *SlSTP2/6/9/13/14/15/18* feature the dominant pattern of four exons and three introns; *SlSTP3/7/17* have three exons and two introns, and *SlSTP1/5/11/12/16* contain five exons. *SlSTP4* (5 exons, 5 introns) and *SlSTP10* (6 exons, 5 introns) possess unique structures, while *SlSTP8* is the most compact with one exon and one intron (Fig. 3a). Such dominant conserved architecture has been previously reported in STP families of pear and cabbage. Genes within identical phylogenetic clades share highly similar structural arrangements, demonstrating that conserved gene architecture is essential for precise pre-mRNA splicing and intact transporter function, whereas structural variations originate from evolutionary intron gain or loss. Ten conserved motifs display obvious clade-specific distribution across the family, providing protein-level evidence for functional divergence among different subgroups (Fig. 3b).

The 18 *SlSTP* scatter across eleven chromosomes, among which seven genes cluster on chromosome 3 into two independent tandem arrays: *SlSTP7/10/13* and *SlSTP14/15/16/17* (Fig. 1). Genes derived from tandem duplication account for 38.9% of the family, and no segmental duplication was identified, revealing that tandem duplication dominates the expansion of the *SlSTP* family, an evolutionary mechanism conserved among STP families of *Arabidopsis*, rice and maize. Paralogous genes *SlSTP14/15/16/17* within the same cluster share nearly identical motif composition, which implies obvious initial functional redundancy shortly after tandem duplication (Fig. 3a). By contrast, genes from distinct clusters show disparate tissue-specific expression patterns. It can be inferred that tandem duplication mainly expands gene dosage, and subsequent promoter sequence variation and cis-element differentiation drive gradual subfunctionalization of duplicated paralogs, as exemplified by distinct cis-regulatory landscapes between closely related *SlSTP1* and *SlSTP10*. Furthermore, extensive syntenic orthologous *STP* pairs between tomato and potato indicate highly conserved chromosomal positioning of *STP* loci during Solanaceae speciation (Fig. 2b).

## Analysis on Transmembrane and Structural Characteristics of SlSTP

Plant monosaccharide transporters belonging to the major facilitator superfamily (MFS) are characterized by 12 conserved transmembrane helices (TMHs), which construct intact substrate-binding pockets and transmembrane channels and serve as the structural basis for substrate recognition and transmembrane transport (Supplemental Table S3). In this study, most SlSTP members including SlSTP1/2/3/6/10/12/15/16 contained 12 TMHs and presented complete secondary structural compositions, fully consistent with the typical topological features of canonical MFS transporters. SlSTP4/5/7/9/11/13 and SlSTP18 had a small number of missing transmembrane segments. According to the amino acid length, physicochemical properties and secondary structure data in Table 1 and Supplemental Table S3, these mild structural variations did not cause dramatic changes to protein spatial conformation. Slight polymorphism of transmembrane regions is a common phenomenon during the gene duplication and evolutionary differentiation of plant STP families, and such variations generally do not hinder the basic monosaccharide transport function of proteins.

Distinct structural defects were observed in SlSTP8/14 and SlSTP17, which differed greatly from most family members. SlSTP17 only had 4 TMHs and possessed an extremely short amino acid sequence of 267 aa, confirming it as a severely truncated protein (Table 1). Its α-helix content ranked the highest across the entire family, indicating that most α-helical structures lost the ability to span the membrane. The massive deletion of transmembrane domains damaged the integrity of substrate-binding pockets and transport channels, which was highly likely to reduce monosaccharide transport efficiency or even lead to partial loss of transport function. SlSTP8 and SlSTP14 also had incomplete transmembrane topology and altered overall spatial skeletons. These structural alterations imply that the three proteins have experienced obvious functional differentiation during long-term evolution. They may either only maintain weak transport activity towards specific monosaccharide substrates, or evolve novel biological functions independent of transmembrane transport. Additionally, SlSTP9 and SlSTP15 had extraordinarily long protein sequences but normal TMH numbers, demonstrating that their extra amino acid residues were distributed in intracellular and extracellular domains rather than transmembrane regions. These non-transmembrane sequences may participate in post-translational modification, protein-protein interaction or dynamic regulation of transport activity.

**Divergent cis-element configuration governs tissue-specific and stress-responsive transcription of SlSTP**

Cis-acting elements in gene promoters are core regulators of gene transcription. In this study, four major categories of cis-elements were identified in the 2000 bp promoter sequences of 18 *SlSTP*, including light-responsive, phytohormone-responsive, stress-responsive and development-related motifs (Fig. 5a). On this basis, we further annotated heat shock-related, sugar signaling-related, flower and fruit development-related functional motifs, revealing a complex and diverse transcriptional regulatory system of the *SlSTP* family. Light-responsive motifs were the most abundant and widely distributed across all promoters (Fig. 5b). As a typical multifunctional element, G-box integrates light signal perception, sugar signal transduction and carbon metabolism, acting as a key link between environmental light and endogenous carbohydrate metabolism. A variety of hormone response elements related to ABA, MeJA, SA, auxin and gibberellin were ubiquitous in *SlSTP* promoters, and these elements cooperatively regulate flower organogenesis and fruit expansion, leading to distinct hormone response patterns among family members. Apart from drought, cold and anaerobic stress elements such as MBS, LTR and ARE, heat stress-related ACE and STRE were also discovered. LTR and TC-rich repeats can respond to both low temperature and high temperature, enabling *SlSTP* to cope with multiple temperature stresses. *SlSTP2* and *SlSTP5* contained a large number of stress-related cis-elements, which corresponded to their strong inducibility under drought, waterlogging, cold and heat stress. Development-related elements including CAT-box, O2-site, chs-CMA1a and circadian motifs participate in meristem development, sugar accumulation, seed formation and secondary metabolism. Given that tomato mature fruit does not form endosperm, the actual function of O2-site needs to be verified via subsequent genetic functional analysis.

Phylogenetic analysis showed that *SlSTP* members within the same clade shared highly conserved cis-element composition and arrangement, while obvious divergence occurred between different phylogenetic subgroups (Fig. 2a; Fig. 5a). *SlSTP15/16/17* had nearly identical cis-element profiles, whereas the closely related paralogs *SlSTP1* and *SlSTP10* showed great differences in element types and copy numbers. Genes in Clade III were rich in pollen-specific motifs, which directly accounted for their predominant expression in floral tissues. During long-term evolution, continuous base mutations in promoter regions altered the combination of cis-elements of *SlSTP* family members, resulting in differentiated transcriptional regulation characteristics. In conclusion, the variation of cis-regulatory elements is the essential molecular reason for the diverse expression patterns in different tissues, differential responses to sugar signals and various abiotic stresses among *SlSTP* family members.

**Organ-preferential divergent expression enables functional partitioning of SlSTP during tomato root, flower and fruit development**

Members of the *SlSTP* family exhibit pronounced organ-specific spatiotemporal expression, and coordinated transcriptional divergence contributes to the developmental regulation of root architecture, floral differentiation and early fruit growth in tomato (Fig. 6a).

Roots accumulate the highest overall transcript abundance of *SlSTP*, with constitutively high expression of *SlSTP1/12/16/17* belonging to Clade II. Functional studies in *Arabidopsis* have validated that orthologs *AtSTP1* and *AtSTP4* facilitate root monosaccharide uptake and internal carbon partitioning (Truernit et al., 1996; Sherson et al., 2000). By analogy, these root-enriched tomato genes are hypothesized to absorb glucose and fructose from rhizosphere to sustain root carbon supply and growth, as well as mediate sugar exchange between plant roots and rhizosphere microorganisms.

Floral tissues constitute the predominant expression site for most *SlSTP*, wherein twelve genes are sharply upregulated at the flower bud stage. Two Clade III members, *SlSTP9/11*, maintain extremely high transcription from budding to full bloom. Their *Arabidopsis* counterparts (*AtSTP9/11*) are pollen-specific transporters importing apoplastic monosaccharides to support pollen maturation and pollen tube elongation (Schneidereit et al., 2003, 2005), implying conserved roles of *SlSTP9/11* in male gametogenesis and fertilization. Other Clade III genes including *SlSTP4/15* display discrete expression across anthers and ovaries to fulfill carbohydrate supply for complete floral development.

Most *SlSTP* are transcriptionally repressed throughout fruit development, while limited paralogs show stage-specific transcription: *SlSTP1* is transiently induced at early fruit expansion, *SlSTP3* maintains steady moderate expression across all fruit stages, and *SlSTP10* only peaks transiently in 1 cm young fruits. Such expression pattern demonstrates that STP-dependent monosaccharide transport primarily drives cell division and expansion in immature fruits. During subsequent fruit ripening and sugar accumulation, SlSUT and SlSWEET become the major contributors to sugar translocation. Collectively, organ-specialized transcriptional programming underpins subfunctionalization of the SlSTP family and accommodates carbon transport demands for distinct tomato organ development.

**Distinct Responses to Biotic/Abiotic Stresses and Stress Regulatory Network of SlSTP**

According to their induction profiles, these genes are sorted into universally responsive, biotic-specific, abiotic-specific and oppositely regulated subgroups, constructing the sugar-transport-dependent regulatory network for tomato stress tolerance.

Samples of nematode infection were collected at sequential time points (7, 14, 21, 28, 35 dpi), corresponding to successive parasitic developmental stages. At early infection (7–14 dpi), only *SlSTP10* was significantly induced. This observation is consistent with recent functional evidence demonstrating that *SlSTP10* acts downstream of the miR396a-*SlGRF8* module and is transcriptionally activated upon root-knot nematode infection to modulate root sugar allocation during tomato-nematode interactions (Sun et al., 2024). The 21 dpi corresponds to critical stages of giant-cell formation and intensive nutrient acquisition of nematodes (Portillo et al., 2013), where *SlSTP1/2/3/7/8/12* peaked synchronously (Fig. 6b). Similar to AtSTP4 delivering hexose toward pathogen-infected tissues (Truernit et al., 1996), these genes presumably supply monosaccharides to feeding sites for nematode development. Several genes including *SlSTP6/7/13/14* were newly upregulated at 35 dpi and may participate in root wound repair and late-stage defense responses. Late-stage upregulation of *SlSTP13* at 35 dpi is associated with root tissue repair, consistent with documented roles of *AtSTP13* in programmed cell death (Nørholm et al., 2006). Constitutive repression of *SlSTP16* throughout infection suggests nematode manipulation of host root carbon export.

All abiotic samples were harvested on the 8th day post-treatment to detect steady-state transcriptional reprogramming after long-term stress acclimation, lacking serial sampling for early-response characterization. Stress-induced genes distributed across roots (61.1%), leaves (44.4%), flowers (33.3%) and stems (16.7%) (Fig. 6c-e). As universal responders, *SlSTP7/12* were differentially upregulated in diverse organs under all three abiotic stresses owing to abundant stress-related cis-elements in promoters. Root-specific strong induction of *SlSTP6/12* under drought facilitates osmotic homeostasis via soluble sugar accumulation, a conserved regulatory mode reported in rice *OsSTP* (Deng et al., 2019). *SlSTP17* was induced in roots under salt but sharply repressed under heat, executing divergent physiological roles across distinct abiotic cues.

Cross-stress comparison identifies *SlSTP7/12* as central regulatory hubs, markedly upregulated at nematode peak stage as well as under all three abiotic treatments; abundant ABA-responsive motifs and JA-responsive motifs in their promoters enable integration of heterogeneous stress signals (Fig. 6b-e). Additional genes (*SlSTP3/6/8/10/13/14*) also respond to both biotic and abiotic challenges. *SlSTP2* is nematode-specific without detectable induction under abiotic conditions, while *SlSTP5/9/17* are exclusively induced under abiotic stresses and classified as abiotic-specific genes. Exceptionally, *SlSTP16* is persistently suppressed during nematode parasitism but significantly induced by drought and salt, indicating opposite physiological functions under disparate stresses.

## Conclusion

In this study, a systematic analysis was performed on the 18 previously reported *SlSTP* in the tomato genome. Phylogenetic analysis classified them into four clades, with Clade I being absent in tomato. Tandem duplications on chromosome 3 were identified as the major driver of family expansion. *SlSTP1*, *SlSTP12*, and *SlSTP16* (Clade II) showed predominant expression in roots, while *SlSTP9* and *SlSTP11* (Clade III) were specifically highly expressed in flowers. Most *SlSTP* were only detectable during early fruit expansion. *SlSTP7* and *SlSTP12* exhibited broad-spectrum responses to both root-knot nematode infection and all three abiotic stresses tested (drought, salt, and heat). Notably, *SlSTP6* and *SlSTP12* were strongly induced in roots under drought stress, with $\log_2$ fold changes exceeding 5. This study is based on transcriptomic and bioinformatic analyses; therefore, the substrate specificity of each SlSTP has not yet been determined by yeast complementation assays, and the developmental and stress-related functions of key genes lack transgenic validation. Furthermore, the upstream transcription factors regulating these genes and the evolutionary mechanism underlying the loss of Clade I in tomato remain unclear. Collectively, this study provides candidate gene resources for sugar metabolism improvement and stress tolerance breeding in tomato.

## Declarations

# Competing interests

The authors declare no competing interests.

# Funding

This work was supported by Beijing Agricultural Science and Technology Project for Rural Revitalization (NY2501010126); Chinese Universities Scientific Fund (2026RC030).

# Author Contribution

S.M. and Y.Q.T.conceived the project; S.M. designed the study; Z.J.L., Y.F.G. and X.Y.W. performed the experiments and collected the data; Z.J.L. and Y.F.G. analyzed and interpreted the data; Y.X.T. provided technical assistance during the experiment; S.M., Y.Q.T., L.Y.S. and X.L. offered valuable suggestions on experiment arrangement and result explanation; Z.J.L., Y.F.G., X.Y.W. and S.M. wrote the drafts. All authors approved the final version of the manuscript.

## Acknowledgement

We appreciate the CAB Public Instrument Platform of China Agricultural University for providing access to CFX96 Real-Time PCR System (Bio-Rad, USA) for qRT-PCR analysis.

## References

1. Afoufa-Bastien D, Medici A, Jeauffre J, Coutos-Thévenot P, Lemoine R, Atanassova R, Laloi M (2010) The vitis vinifera sugar transporter gene family: phylogenetic overview and macroarray expression profiling. BMC Plant Biol 10:245–266. https://doi.org/10.1186/1471-2229-10-245
2. Bhattarai S, Harvey J, Djidonou D, Leskovar D (2021) Exploring morpho-physiological variation for heat stress tolerance in tomato. Plants 10:347–368. https://doi.org/10.3390/plants10020347
3. Büttner M (2010) The *arabidopsis* sugar transporter (AtSTP) family: an update. Plant Biol 12:35–41. https://doi.org/10.1111/j.1438-8677.2010.00383.x
4. Caseys C (2018) Regulatory divergence in the stress response of tomato. Plant Cell 30:1381–1380. https://doi.org/10.1105/tpc.18.00433
5. Chen L-Q, Cheung LS, Feng L, Tanner W, Frommer WB (2015) Transport of sugars. Annu Rev Biochem 84:865–894. https://doi.org/10.1146/annurev-biochem-060614-033904
6. Deng X, An B, Zhong H, Yang J, Kong W, Li Y (2019) A novel insight into functional divergence of the MST gene family in rice based on comprehensive expression patterns. Genes 10:239–256. https://doi.org/10.3390/genes10030239
7. Devi B, Dogra V, Mali S, Nayyar H, Rathour R, Sharma KD (2025) Sugar transporter protein (STP) genes in chickpea. Trop Plant Biol 18:50–66. https://doi.org/10.1007/s12042-025-09421-4
8. Geiger D (2020) Plant glucose transporter structure and function. Pflüg Arch - Eur J Physiol 472:1111–1128. https://doi.org/10.1007/s00424-020-02449-3
9. Kong W, An B, Zhang Y, Yang J, Li S, Sun T, Li Y (2019) Sugar transporter proteins (STPs) in gramineae crops: comparative analysis, phylogeny, evolution, and expression profiling. Cells 8:560–574. https://doi.org/10.3390/cells8060560
10. Li YM, Wang J, Wang P, Shi K (2022) Function of sugar transporter SlSTP2 in tomato defense against bacterial leaf spot. Scientia Agric Sin 55:3144–3154. https://doi.org/10.3864/j.issn.0578-1752.2022.16.007
11. Liu H, Li C, Qiao L, Hu L, Wang X, Wang J, Ruan X, Yang G, Yin G, Wang C, Sun Z, Ma K, Li L (2021) The sugar transporter family in wheat (*triticum aestivum*. L): genome-wide identification, classification, and expression profiling during stress in seedlings. PeerJ 9:e11371. https://doi.org/10.7717/peerj.11371
12. Liu Q, Dang H, Chen Z, Wu J, Chen Y, Chen S, Luo L (2018) Genome-wide identification, expression, and functional analysis of the sugar transporter gene family in cassava (*manihot esculenta*). Int J Mol Sci 19:987–1005. https://doi.org/10.3390/ijms19040987
13. Liu T, Bao C, Ban Q, Wang C, Hu T, Wang J (2022) Genome-wide identification of sugar transporter gene family in brassicaceae crops and an expression analysis in the radish. BMC Plant Biol 22:245–260. https://doi.org/10.1186/s12870-022-03629-2
14. Ma Y, Zhou Z, Cao H, Zhou F, Si H, Zang J, Xing J, Zhang K, Dong J (2023) Identification and expression analysis of sugar transporter family genes reveal the role of ZmSTP2 and ZmSTP20 in maize disease resistance. J Integr Agric 22:3458–3473. https://doi.org/10.1016/j.jia.2022.12.014
15. Mia MS, Nayan SB, Islam MN, Talukder MEK, Hasan MS, Riazuddin M, Shadhin MST, Hossain MN, Wani TA, Zargar S, Rabby MG (2025) Genome-wide exploration: evolution, structural characterization, molecular docking, molecular dynamics simulation and expression analysis of sugar transporter (ST) gene family in potato (*solanum tuberosum*). Comput Biol Chem 117:108402. https://doi.org/10.1016/j.compbiolchem.2025.108402
16. Nørholm MHH, Nour-Eldin HH, Brodersen P, Mundy J, Halkier BA (2006) Expression of the *Arabidopsis* high-affinity hexose transporter STP13 correlates with programmed cell death. FEBS Lett 580:2381–2387. https://doi.org/10.1016/j.febslet.2006.03.064
17. Portillo M, Cabrera J, Lindsey K, Topping J, Andrés MF, Emiliozzi M, Oliveros JC, García-Casado G, Solano R, Koltai H, Resnick N, Fenoll C, Escobar C (2013) Distinct and conserved transcriptomic changes during nematode-induced giant cell development in tomato compared with *Arabidopsis*: a functional role for gene repression. New Phytol 197:1276–1290. https://doi.org/10.1111/nph.12121
18. Reimer JJ, Thiele B, Biermann RT, Junker-Frohn LV, Wiese-Klinkenberg A, Usadel B, Wormit A (2021) Tomato leaves under stress: a comparison of stress response to mild abiotic stress between a cultivated and a wild tomato species. Plant Mol Biol 107:177–206. https://doi.org/10.1007/s11103-021-01194-0
19. Reuscher S, Akiyama M, Yasuda T, Makino H, Aoki K, Shibata D, Shiratake K (2014) The sugar transporter inventory of tomato: genome-wide identification and expression analysis. Plant Cell Physiol 55:1123–1141. https://doi.org/10.1093/pcp/pcu052
20. Schneidereit A, Scholz-Starke J, Büttner M (2003) Functional characterization and expression analyses of the glucose-specific AtSTP9 monosaccharide transporter in pollen of *arabidopsis*. Plant Physiol 133:182–190. https://doi.org/10.1104/pp.103.026674
21. Schneidereit A, Scholz-Starke J, Sauer N, Büttner M (2005) AtSTP11, a pollen tube-specific monosaccharide transporter in *arabidopsis*. Planta 221:48–55. https://doi.org/10.1007/s00425-004-1420-5
22. Sherson SM, Hemmann G, Wallace G, Forbes S, Germain V, Stadler R, Bechtold N, Sauer N, Smith SM (2000) Monosaccharide/proton symporter AtSTP1 plays a major role in uptake and response of *Arabidopsis* seeds and seedlings to sugars. Plant J 24:849–857. https://doi.org/10.1111/j.1365-

313X.2000.00935.x

23. Sun L, Zhu M, Zhou X, Gu R, Hou Y, Li T, Huang H, Yang R, Wang S, Zhao W (2024) The miR396a–SlGRF8 module regulates sugar accumulation in the roots via SlSTP10 during the interaction between root-knot nematodes and tomato plants. J Integr Plant Biol 66:2701–2715. https://doi.org/10.1111/jipb.13794
24. Truernit E, Schmid J, Epple P, Illig J, Sauer N (1996) The sink-specific and stress-regulated *arabidopsis* STP4 gene: enhanced expression of a gene encoding a monosaccharide transporter by wounding, elicitors, and pathogen challenge. Plant Cell 8:2169–2182. https://doi.org/10.1105/tpc.8.12.2169
25. Wang Y, Shi C, Ge P, Li F, Zhu L, Wang, Yaru, Tao J, Zhang X, Dong H, Gai W, Wang F, Ye Z, Grierson D, Xu W, Zhang Y (2023) A 21-bp InDel in the promoter of *STP1* selected during tomato improvement accounts for soluble solid content in fruits. Hortic Res 10:uhad009. https://doi.org/10.1093/hr/uhad009
26. Wei H, Liu J, Zheng J, Zhou R, Cheng Y, Ruan M, Ye Q, Wang R, Yao Z, Zhou G, Deng M, Chen Y, Wan H (2020) Sugar transporter proteins in *capsicum*: identification, characterization, evolution and expression patterns. Biotechnol Biotechnol Equip 34:341–353. https://doi.org/10.1080/13102818.2020.1749529
27. Xiao Q, Li Z, Wang Y, Hou X, Wei X, Zhao X, Huang L, Guo Y, Liu Z (2022) Genome-wide identification, expression and functional analysis of sugar transporters in sorghum (*sorghum bicolor* L). J Integr Agric 21:2848–2864. https://doi.org/10.1016/j.jia.2022.07.034
28. Zhang W, Wang S, Yu F, Tang J, Yu L, Wang H, Li J (2019) Genome-wide identification and expression profiling of sugar transporter protein (STP) family genes in Cabbage (*Brassica oleracea* var. capitata L.) reveals their involvement in clubroot disease responses. Genes 10:71. https://doi.org/10.3390/genes10010071

## Figures

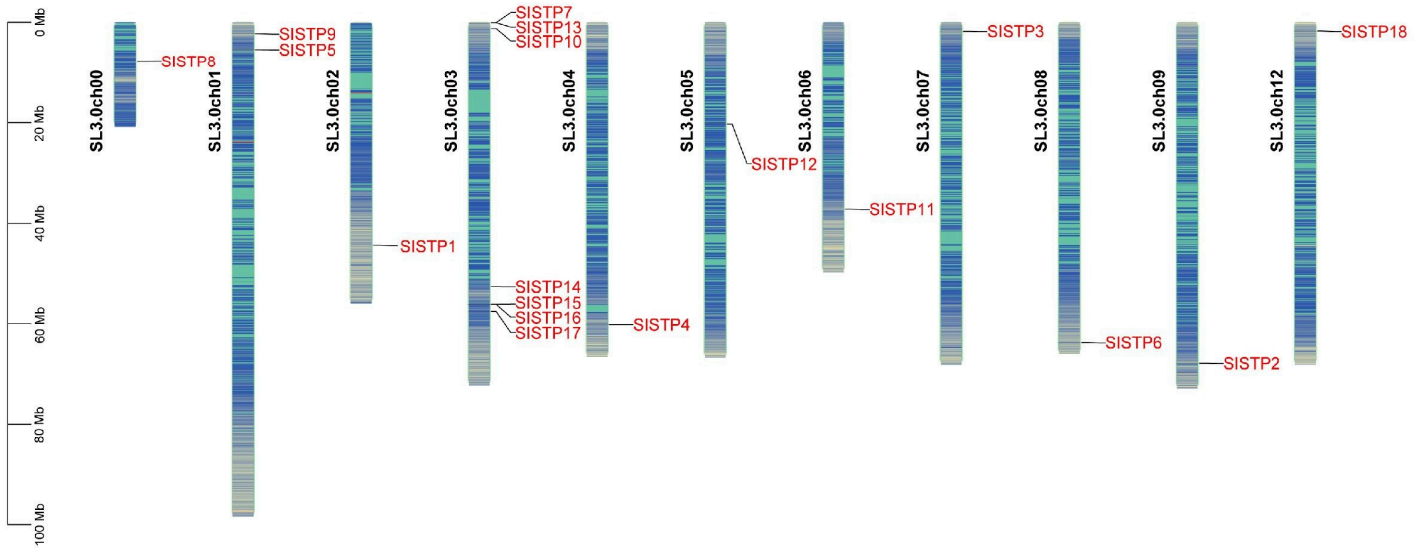



**Figure 1**

**Chromosomal localization and distribution of the *SlSTP* family.**

The vertical scale on the left represents the physical length of the chromosomes. The vertical bar charts represent each chromosome of the tomato, with the chromosome names labeled on their left side. The color gradient (from blue to yellow green) inside the bars reflects the gene density in that chromosomal segment. The red text and connecting lines indicate the specific physical positions of the 18 *SlSTP* on each chromosome.

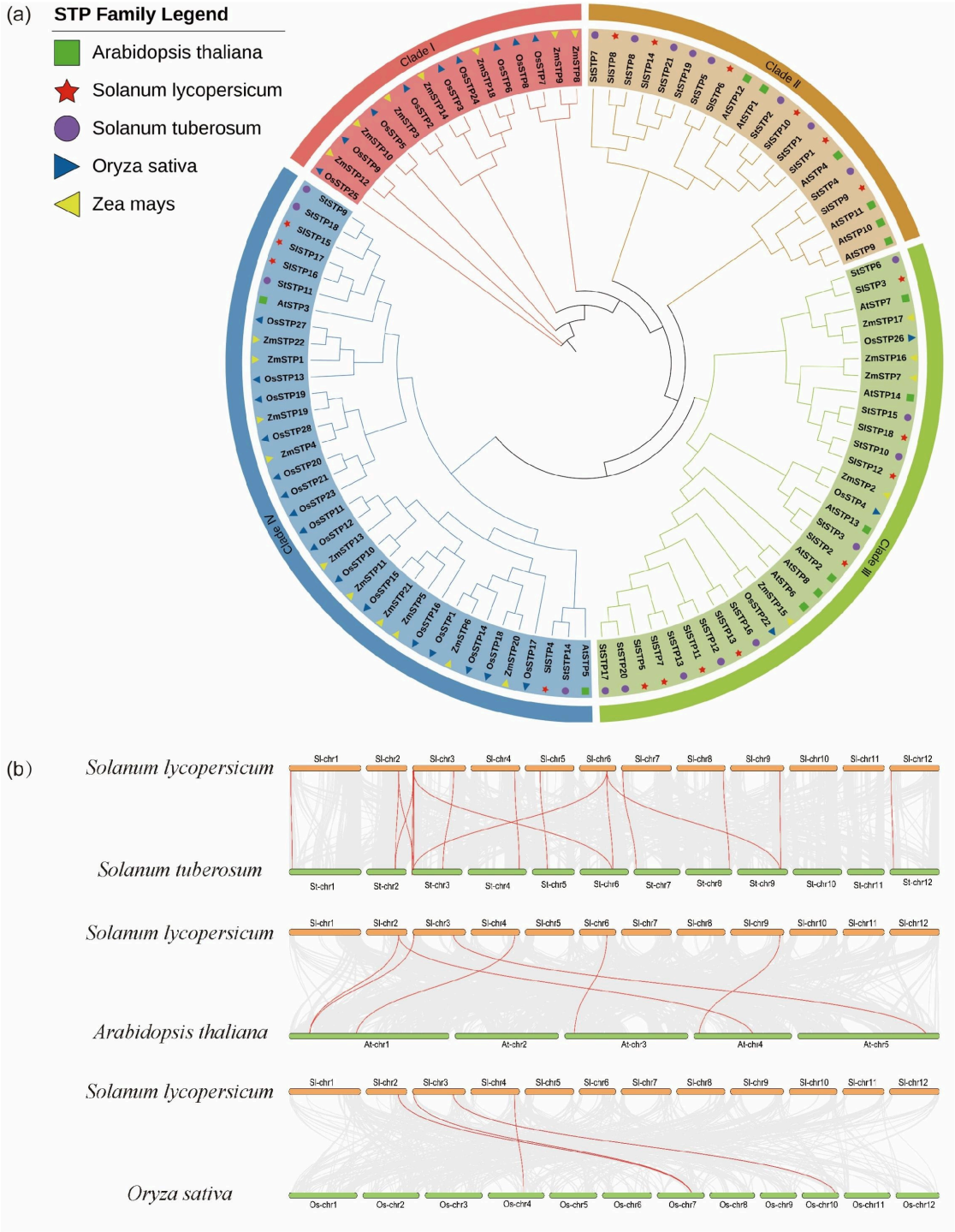



**Figure 2**

**Phylogenetic and collinearity analysis of STP families in tomato and other representative plants.**

(a) Phylogenetic tree of STP from tomato, potato, *Arabidopsis thaliana*, rice, and maize. The outer fan-shaped regions in different colors represent different phylogenetic clades (Clade I-IV). Different shapes and colors at the ends of the branches represent different species (green square: *Arabidopsis thaliana*; red pentagram: tomato; purple circle: potato; blue triangle: rice; yellow triangle: maize).

(b) Genome collinearity analysis between tomato and potato, *Arabidopsis thaliana* and rice. The gray background lines represent collinear blocks at the whole-genome level between species, while the red connecting lines specifically refer to orthologous collinear gene pairs of STP between tomato and other species.

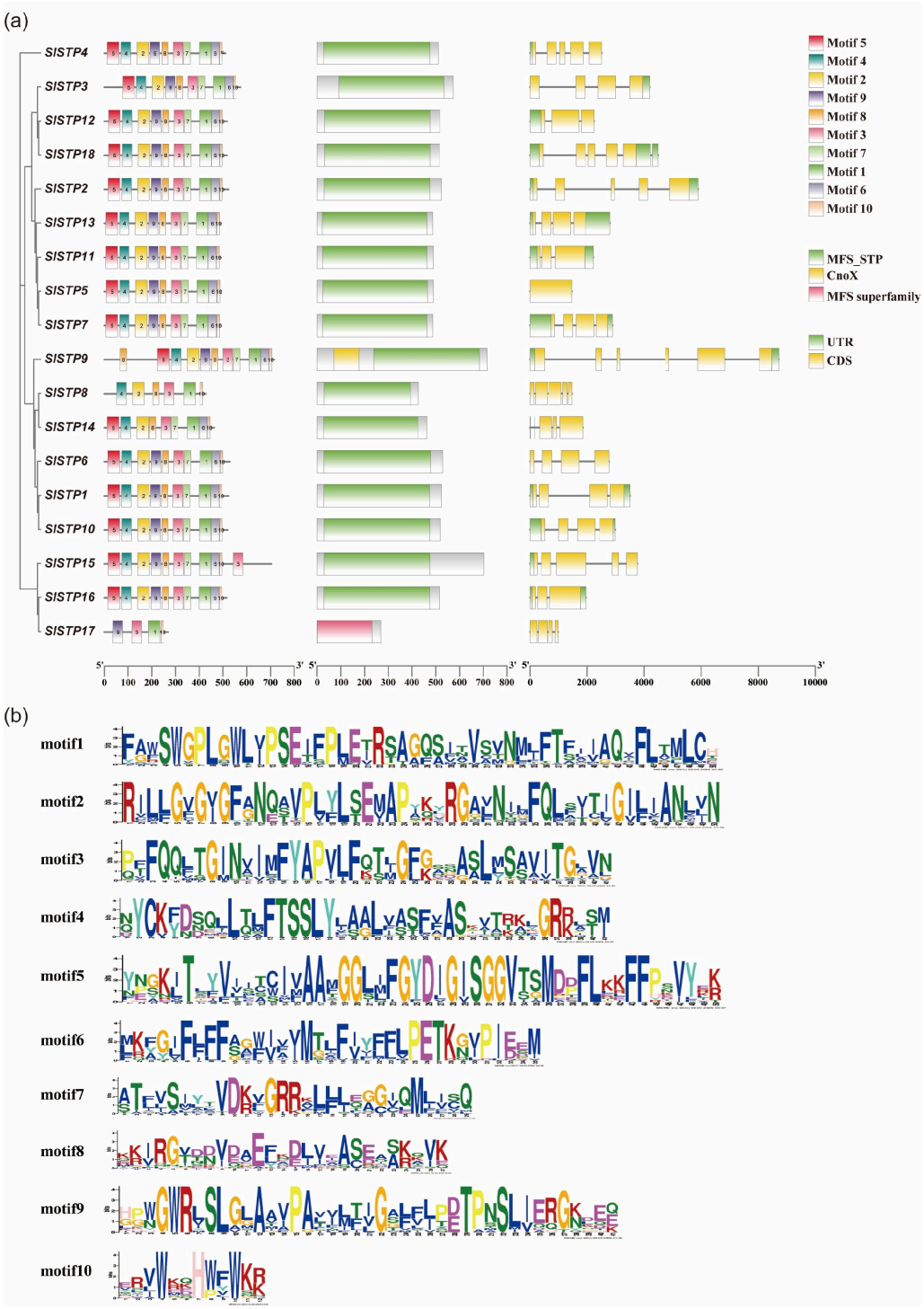



**Figure 3**

**Gene structure and conserved motif characterization of *SlSTP* family.**

(a) Exon-intron organization and distribution of conserved motifs (Motif 1–10) across 18 *SlSTP*. Colored boxes indicate distinct conserved motifs; black horizontal lines represent introns; yellow boxes correspond to coding sequences (CDS), and green boxes denote untranslated regions (UTR). The scale bar at the bottom shows the sequence length.

(b) Sequence logos of the ten conserved motifs

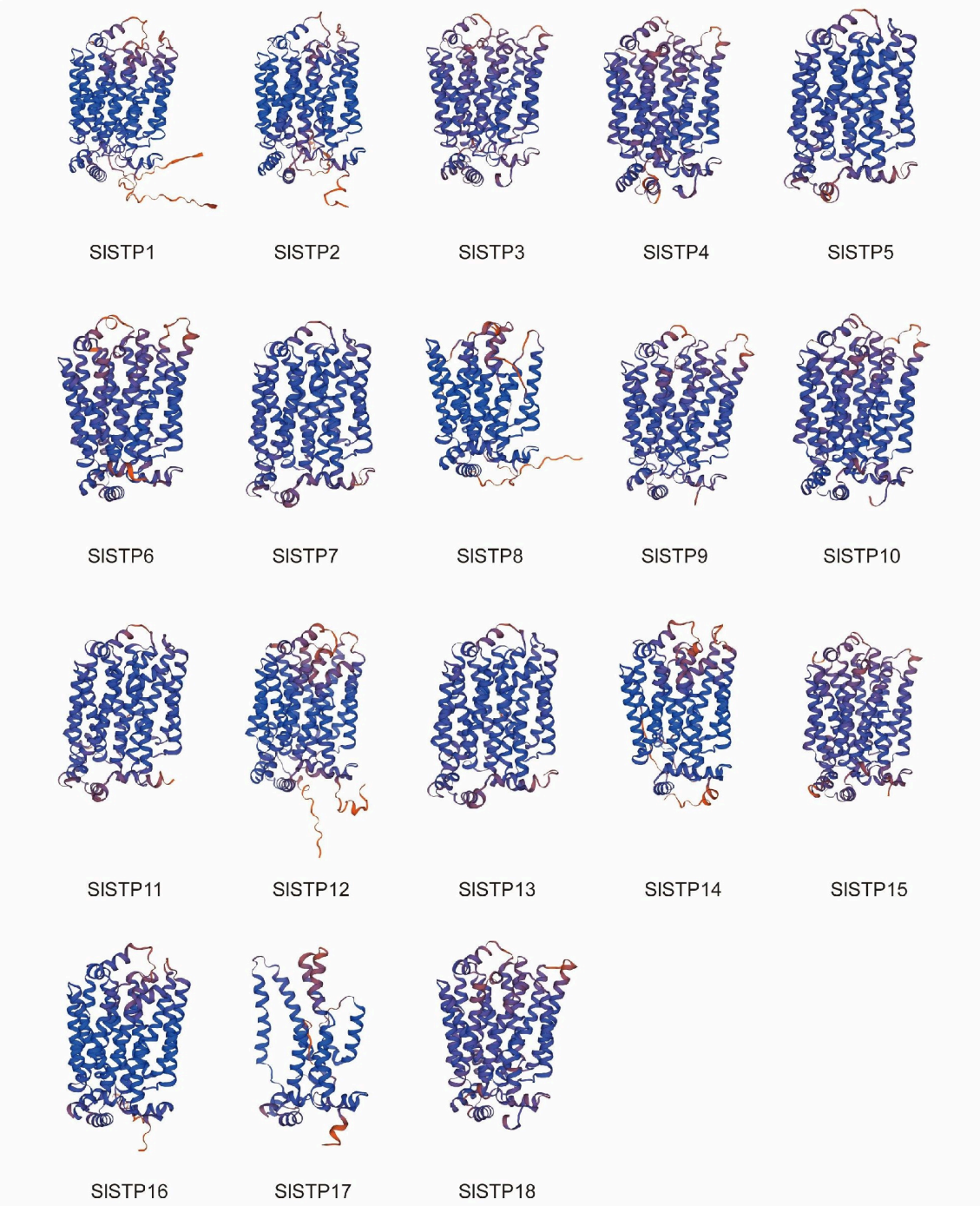



**Figure 4**

**Homology-based tertiary structure modeling of SISTP.**

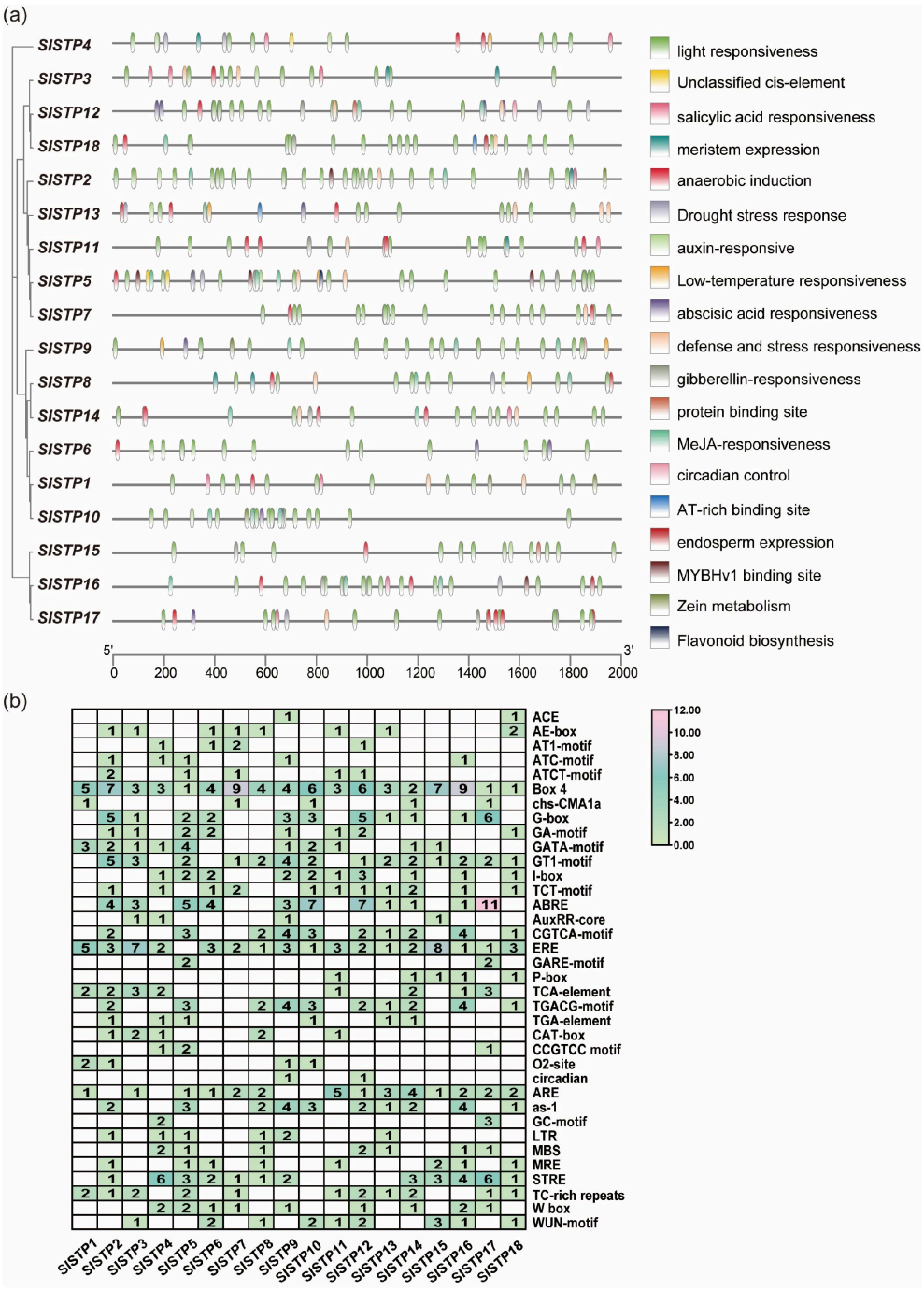



**Figure 5**

**Analysis of cis-acting elements in the promoters of *SlSTP*.**

(a) Types and positional distribution of cis-acting elements in the promoter regions of *SlSTP*.

(b) Quantity statistics of major cis-acting elements in *SlSTP* promoters.

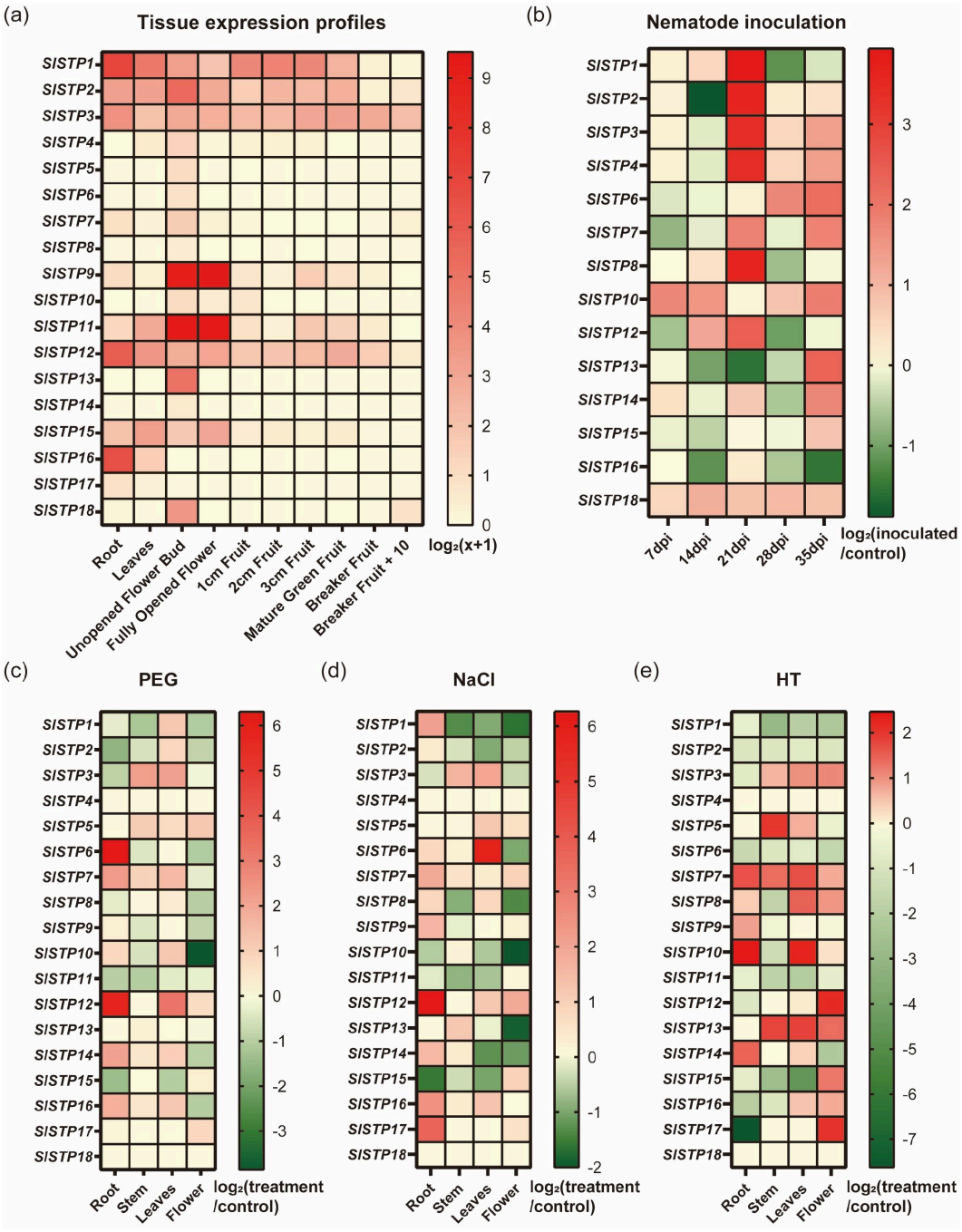



**Figure 6**

**Expression heatmaps of *SlSTP* in various tissues and under root-knot nematode infection and abiotic stresses.**

(a) Relative expression of *SlSTP*in roots, stems, leaves, flowers and fruits at distinct developmental stages; raw expression values were transformed by $\log_2(x+1)$.

(b) Fold changes of *SlSTP* at 7, 14, 21, 28 and 35 days post inoculation (dpi), calculated as $\log_2$ (inoculated/control).

(c–e) Expression fold changes under PEG-simulated drought, NaCl-triggered salt stress and high temperature (HT), respectively, with values calculated by $\log_2$ (treatment/control). Red indicates high expression or upregulation, and green represents low expression or downregulation.

## Supplementary Files

This is a list of supplementary files associated with this preprint. Click to download.

- Supplementaltables.docx
- Supplementalfigure.pdf